



ELSEVIER

Contents lists available at ScienceDirect

## Applied Thermal Engineering

journal homepage: [www.elsevier.com/locate/apthermeng](http://www.elsevier.com/locate/apthermeng)

Research Paper

## Experimental investigation of R410A and R32 falling film evaporation on horizontal enhanced tubes

Pu-Hang Jin, Chuang-Yao Zhao, Wen-Tao Ji, Wen-Quan Tao\*

Key Laboratory of Thermo-Fluid Science and Engineering, Ministry of Education, School of Energy and Power Engineering, Xi'an Jiaotong University, Xi'an 710049, PR China

## HIGHLIGHTS

- Falling film evaporation with nucleating boiling are experimentally studied for R32 and R410A on four doubly enhanced tubes.
- HTC exhibits two stages with decrease of film flow rate, a quasi-plateau stage and a sharp-decrease stage.
- HTCs increase with heat flux progressively before reaching the partial dryout regime.
- The integrated-fin tube performs best among the four enhanced tubes tested.

## ARTICLE INFO

## Keywords:

Falling film evaporation  
Plain tube  
Enhanced tubes  
Nucleate boiling heat transfer  
R410A  
R32

## ABSTRACT

In this study, heat transfer performance on horizontal copper tubes of high pressure refrigerants R32 and R410A was investigated. An integrated fin (condensation enhanced) tube and three boiling enhanced tubes with 3-D different enhancement structures were tested. A plain tube was also tested for comparison. Effects of film flow rate, saturation temperature and heat flux on the falling film heat transfer coefficients were investigated. A tube bundle comprised of 6 enhanced boiling tubes was also tested to find the bundle effect. Experiments were carried out at saturation temperatures of 6, 10 and 16 °C, heat fluxes from 20 to 150 kW·m<sup>-2</sup> and film flow rates from 0.01 kg·m<sup>-1</sup>·s<sup>-1</sup> to 0.14 kg·m<sup>-1</sup>·s<sup>-1</sup>. It is found that the effect of film Reynolds number on HTCs of enhanced tubes can be separated into two regimes, a quasi-plateau regime and a sharp decrease regime. HTCs increase with heat flux. Increase of saturation temperature has negligible effect on enhanced tubes as well as the tube bundle. The integrated fin tube performs best among the tubes tested. As a whole, R410A is inferior than R32. Tubes positioned below the top row possess the similar variation trend of HTCs with that of the first row but suffer an earlier dryout.

## 1. Introduction

Evaporator is an indispensable facility of a refrigeration and heat pump system. Several types of evaporators have been proposed and adopted, including flooded type (pool boiling), dried type and the falling-film type evaporator. Despite the fact that falling-film type evaporator was initially patented in 1888 [1], it was not a hot research topic until 1970s because of the oil crisis. From then on, it has been widely used in petrochemical industry, food processing, desalination industry and ocean thermal energy conversion system. With the environmental problems of ozone depletion and global warming becoming more and more serious, the usage of HCFCs in refrigeration and air-conditioning industry came into the eyes of the public all over the world. Montreal's Protocol and later revisions prompted the phasing

out of CFCs which in turn stimulated the usage of falling-film type evaporator in the field of refrigeration, air-conditioning and heat pump for its minuscule liquid inventory compared with the flooded type. Apart from that, falling film evaporator exhibits several other advantages over pool boiling evaporator, such as: higher heat transfer coefficients can be achieved, boiling temperature increase caused by hydrostatic head can be avoided, size of evaporator can be reduced and oil removal from the system is made easier. For these reasons, falling-film evaporator is a potential substitute for pool boiling evaporator. Fig. 1 shows its schematic diagram.

A large number of technical papers about the falling film evaporation have been published in the past several decades, for the simplicity of presentation, only three representative review papers are mentioned below. Ribatski and Jacobi [3] made a comprehensive and critical

\* Corresponding author.

E-mail address: [wqtao@mail.xjtu.edu.cn](mailto:wqtao@mail.xjtu.edu.cn) (W.-Q. Tao).





simplicity of comparison between different refrigerants. Compared with R134a and R123 tested in [25], R32 owns lower GWP (Global Warming Potential). In addition, test will also be conducted for a tube bundle which was not investigated in Ref. [25].

In the following, the test facility will be introduced first, followed by data reduction and uncertainty analysis, then test results will be presented in details. Finally some conclusions will be drawn.

## 2. Experimental setup and tested tubes

The experimental system has three major circulation loops which are chilled (hot) water circuit, chilling (cold) water circuit and refrigerant circuit. Liquid refrigerant is stored at the bottom of the condenser, during operation, liquid refrigerant is pumped to the top of the

evaporator and enters the liquid distributor. Then liquid refrigerant is distributed onto the tube's outer surface to absorb the heat of chilled water inside the tube and evaporates. Refrigerant vapor flows back to the condenser and condenses outside the outer surfaces of the tubes within which chilling water flows. The schematic diagram of the test facility is shown in Fig. 2.

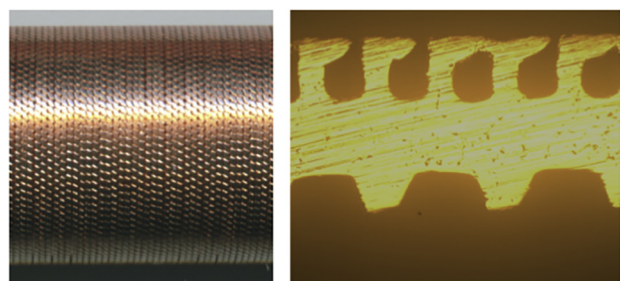
Volume flow rate of chilled and chilling water and mass flow rate of liquid refrigerant are measured with electromagnetic flow meter. A digital pressure gauge is employed to measure the pressure in the evaporator. RTDs are installed at the inlet and outlet of the water to measure the temperature differences. Specifications of measurement instruments are listed in Table 1.

The liquid distributor consists of a preliminary and a secondary distributors. They are two rectangular stainless steel boxes but the top plate of the second one is open-ended. The liquid level in the second box varies with film flow rate which makes the liquid refrigerant flow under gravity. For both boxes, orifices with diameter of 2.0 mm and spacing of 20.0 mm are drilled at the bottom surfaces.

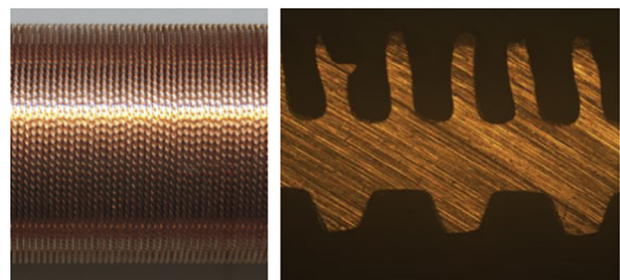
Four enhanced tubes with different enhanced structures are tested on the experimental system. They all have 3-D fins on the outer surface and spiral ribs inside the tube to enhance water side heat transfer. Specifications of enhanced tubes are listed in Table 2 and geometries and scanning pictures of the 3-D fins are shown in Fig. 3. A plain tube is also tested for comparison.

Configuration of the tube bundle is demonstrated in Fig. 4, where the four semi-dummy tubes and one dummy tube is arranged in the tube bundle to simulate the triangular-pitch tube bundle. During the tests, there was no water inside dummy tubes which meant no heat transfer for these tubes. The bottom of the liquid distributor is equipped by two half tubes right above tube No. 5 and No. 9. The two half tubes have a continuous slit along the axial direction to make the liquid refrigerant in the distributor flow through them to tubes No. 5 and No. 9. Tubes in the bundle have the same enhanced structure with tube No. 3. The vertical and horizontal tube pitches are 22.5 mm and 19.5 mm respectively.

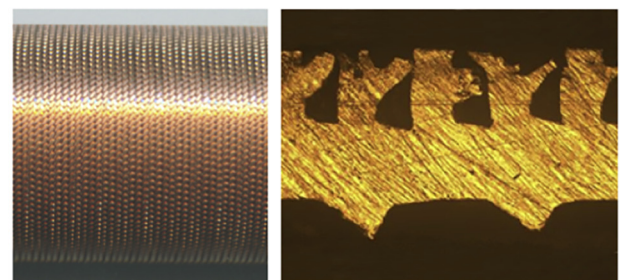
High pressure refrigerants, R32 and R410A, are used as the working fluids. Experimental measurements are carried out for each single tube individually. The ranges of working conditions are listed in Table 3. During the test, the pressures both at the top and the bottom of the evaporator are measured with two digital pressure gauges, and their difference is within the precision of the pressure gauge which indicates that the pressure drop of falling film evaporation within the evaporator is negligible. In addition, the corresponding saturated temperature corresponds well with the liquid refrigerant temperature in the condenser/reservoir. The difference between them (pressure-corresponding saturation temperature and liquid temperature in reservoir) is within 0.1 °C.



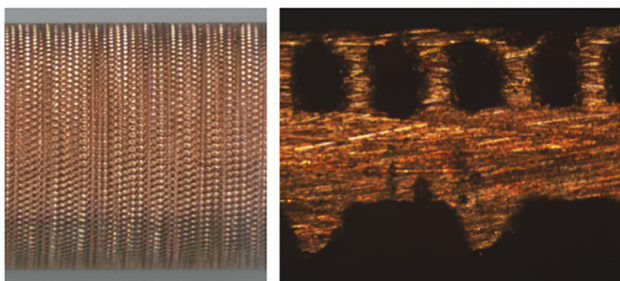
Tube No.1



Tube No.2



Tube No.3



Tube No.4

Fig. 3. Scanning pictures of enhanced surfaces [25].

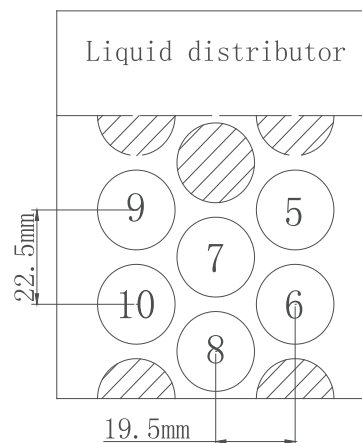


Fig. 4. Tube bundle layout.

**Table 3**  
Experimental conditions for Wilson plot and falling film evaporation.

	Wilson plot	Falling film evaporation
$T_{sat}$ (°C)	6	6, 10, 16
$q$ (kW·m <sup>-2</sup> )	40	20–150
$V_{water}$ (m·s <sup>-1</sup> )	0.7–3.3	2
$\Gamma$ (kg·m <sup>-1</sup> ·s <sup>-1</sup> )	0.08	0.01–0.14

**Table 4**  
Uncertainties of outside heat transfer coefficients.

Tube number	Uncertainty of $h_o$		
	$q$		
	20 kW·m <sup>-2</sup>	40 kW·m <sup>-2</sup>	60 kW·m <sup>-2</sup>
Plain	15.4%	19.6%	24.0%
No. 1	13.0%	13.6%	14.3%
No. 2	19.3%	18.4%	20.2%
No. 3	14.2%	16.2%	15.4%
No. 4	15.1%	15.1%	14.2%

**Table 5**  
Enhanced factors of water side heat transfer coefficients.

Tube number	1	2	3	4	–	–
$c_i$	3.011	2.872	3.122	3.423	–	–
Tube number	5	6	7	8	9	10
$c_i$	3.122	3.22	3.0	3.22	3.39	3.407

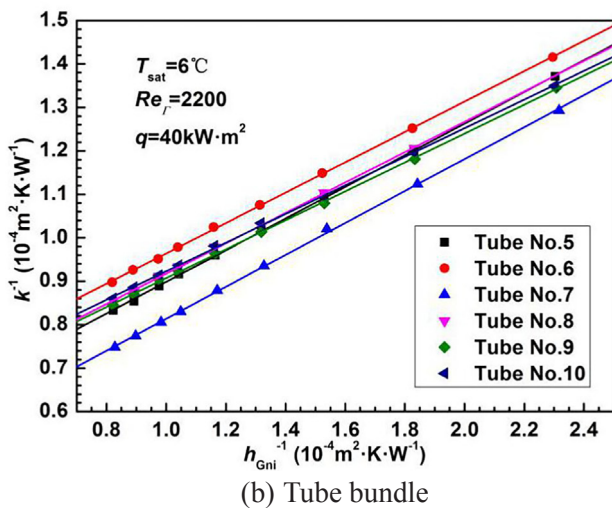
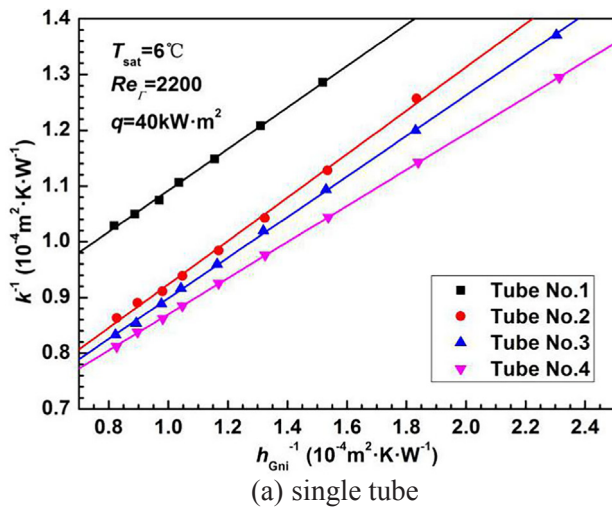


Fig. 5. Variation of  $k^{-1}$  with  $h_{Gni}^{-1}$  for single tube and the tube bundle.

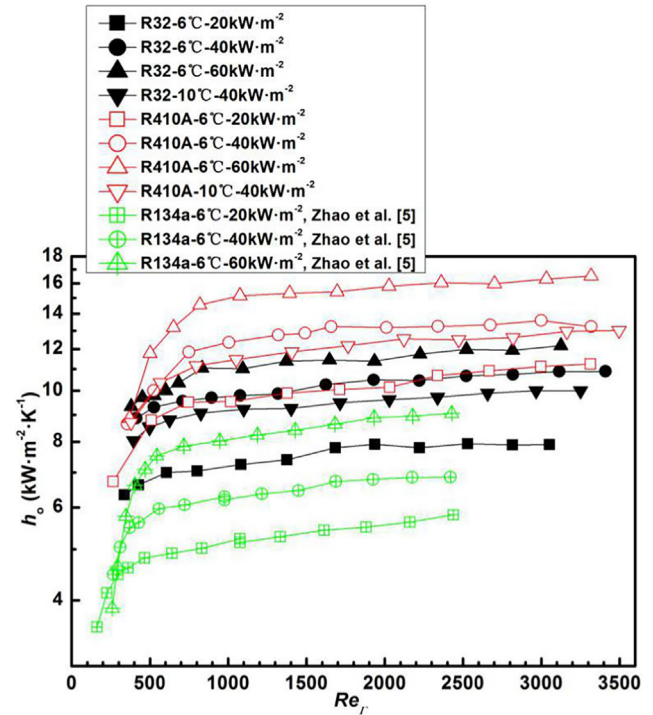


Fig. 6. Variation of falling film evaporation HTCs with film Reynolds number for single plain tube.

### 3. Data reduction and uncertainty analysis

#### 3.1. Heat transfer rate and heat balance

Heat dissipated by the chilled water and absorbed by the chilling water is calculated by Eqs. (1) and (2) respectively:

$$\phi_e = \dot{m}_e c_p (T_{c,in} - T_{c,out}) \quad (1)$$

$$\phi_c = \dot{m}_c c_p (T_{c,out} - T_{c,in}) \quad (2)$$

where  $\dot{m}_e$  and  $\dot{m}_c$  are mass flow rate of chilled water and chilling water respectively,  $c_p$  is the specific heat capacity of water inside the tube.

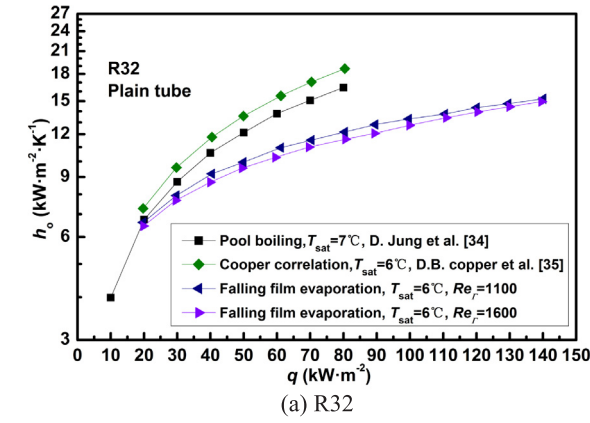
Following heat balance requirement of the system should be satisfied:

$$(\phi_e + \phi_p - \phi_c) / \phi_r \leq 5\% \quad (3)$$

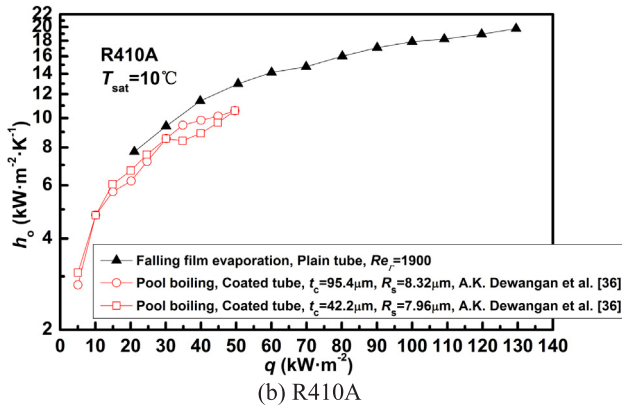
where  $\phi_p$  is the power of the canned motor pump which is immersed in the bulk of liquid refrigerant, 1.5 kW;  $\phi_r$  is the reference heat transfer rate, defined by Eq. (4):

$$\phi_r = (\phi_e + \phi_c - \phi_p) / 2 \quad (4)$$

For all the test data presented in this paper, heat balance deviation is less than 5% which ensures the reliability of determining the overall heat transfer coefficients in next part.



(a) R32



(b) R410A

Fig. 7. HTCs comparison between FFE and PB on plain surfaces.

### 3.2. Overall heat transfer coefficients

The overall heat transfer coefficients of the tested tubes can be expressed by Eq. (5):

$$k = \frac{\phi_e}{A_o \Delta T_{LMTD}} \quad (5)$$

where  $\Delta T_{LMTD}$  is the logarithm mean temperature difference between water and refrigerant saturation temperature.

$\Delta T_{LMTD}$  is defined by Eq. (6).

$$\Delta T_{LMTD} = \frac{|T_{e,in} - T_{e,out}|}{\ln[(T_{e,in} - T_{sat}) / (T_{e,out} - T_{sat})]} \quad (6)$$

where  $T_{sat}$  is the saturation temperature of the refrigerant.

### 3.3. Water side heat transfer coefficients

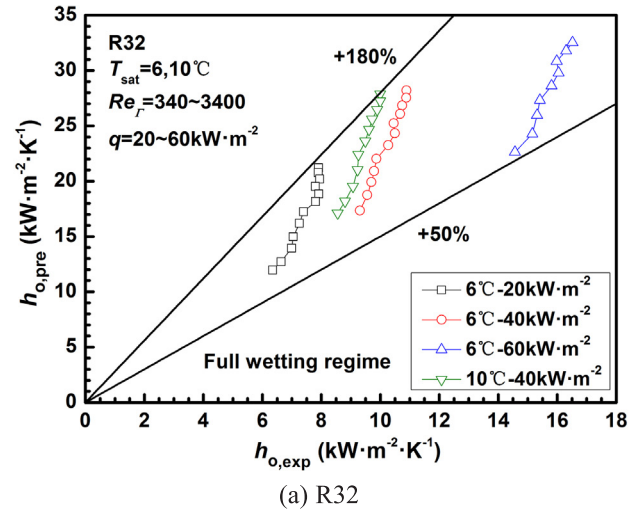
By the thermal resistance analysis, the overall thermal resistance can be expressed as Eq. (7):

$$\frac{1}{k} = \frac{1}{h_o} + R_w + R_f + \frac{1}{h_i} \frac{D_o}{D_i} \quad (7)$$

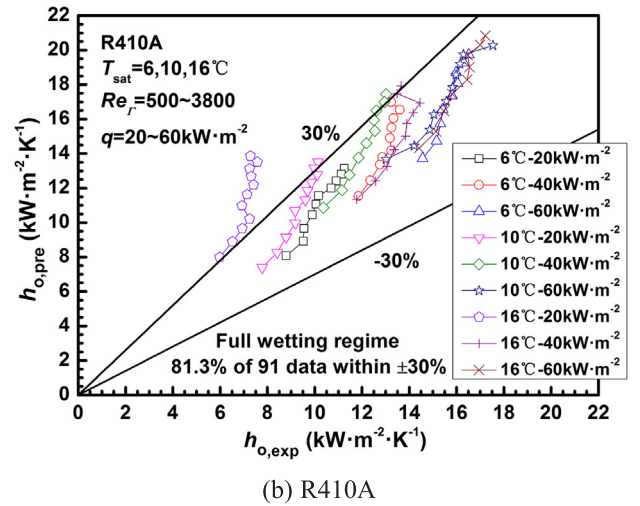
where  $D_i$  and  $D_o$  are the inner and outer diameter of the test tubes,  $R_w$  is the thermal resistance of the tube wall,  $h_i$  is the water side convective heat transfer coefficient and  $R_f$  is the fouling thermal resistance. Since the tested tubes have been cleaned before installation, fouling thermal resistance is neglected in this study.

For the tubes with internal enhancement structures, convective heat transfer coefficients between water and internal surfaces can be expressed by Eq. (8):

$$h_i = c_i h_{Gni} \quad (8)$$



(a) R32



(b) R410A

Fig. 8. Comparison of HTCs between experimental and prediction results [5]

where  $c_i$  is enhanced factor of the internal surface, obtained by Wilson plot method, which is described in detail by Yang and Tao [26]. Gnielinski correlation [27,28] is adopted to calculate the heat transfer coefficients of the plain internal surface,  $h_{Gni}$ .

### 3.4. Shell side heat transfer coefficients

Hence, shell-side heat transfer coefficient can be determined by Eq. (9):

$$h_o = \left[ \frac{1}{k} - \frac{1}{h_i} \frac{D_o}{D_i} - R_w \right]^{-1} \quad (9)$$

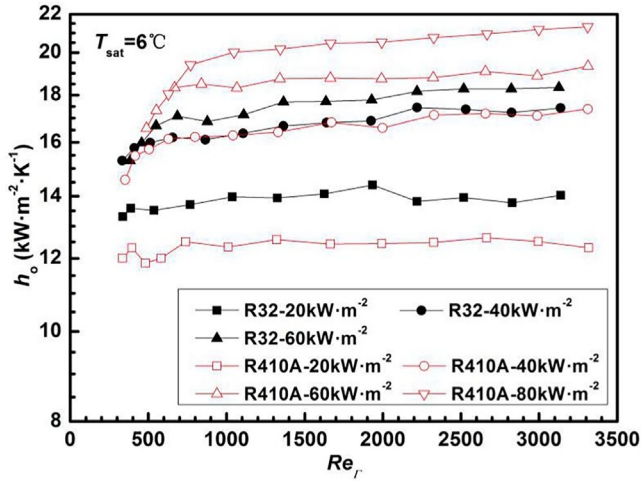
### 3.5. Heat flux, film Reynolds number and average HTCs of single tube and the tube bundle

Heat flux in this paper is the area-averaged heat flux on the outer surface of the tube tested:

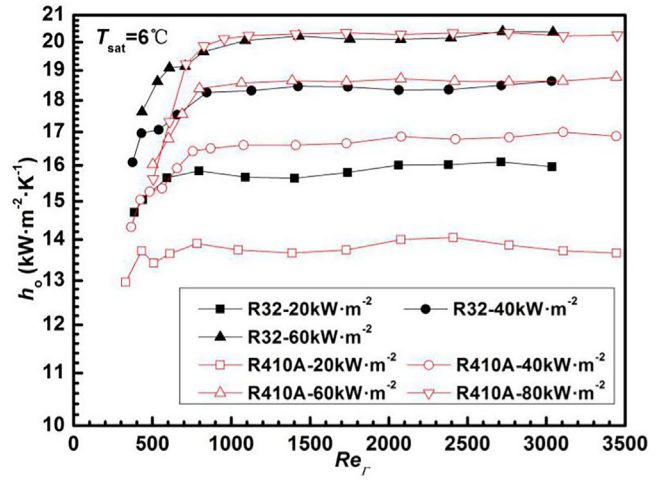
$$q = \frac{\phi_e}{A_o} \quad (10)$$

where  $\phi_e$  is heat transfer rate of the tested tube,  $A_o$  is the outer surface area of the tested tube. For the tube bundle, the heat flux of tube No. 9 is taken as the heat flux of the tube bundle.

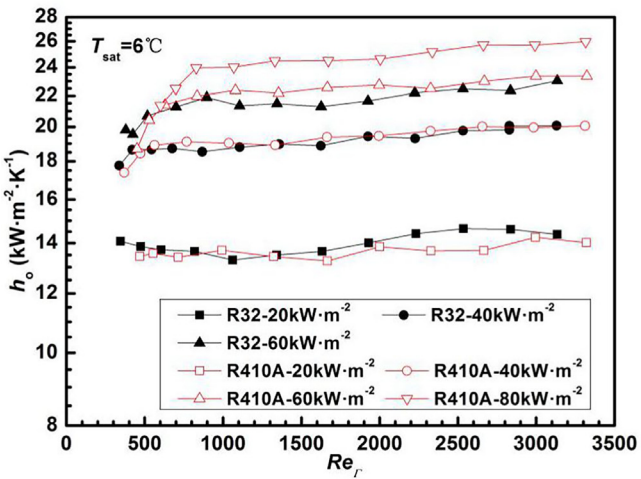
Film Reynolds number is defined by Eq. (11):



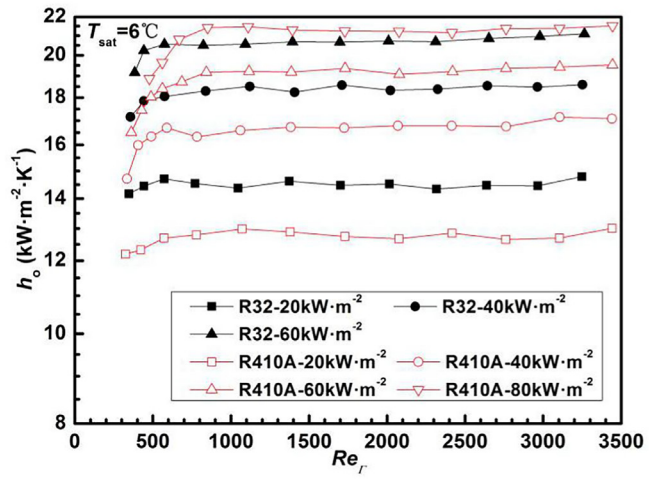
(a) Tube No.1



(c) Tube No.3



(b) Tube No.2



(d) Tube No.4

Fig. 9. Falling film evaporation HTC of R410A and R32 on enhanced tubes.

$$Re_f = \frac{4\Gamma}{\mu_1} \quad (11)$$

where  $\Gamma$  ( $\text{kg}\cdot\text{m}^{-1}\cdot\text{s}^{-1}$ ) is the film flow rate on one side of the tested tube per unit length,  $\mu_1$  ( $\text{kg}\cdot\text{m}^{-1}\cdot\text{s}^{-1}$ ) is the dynamic viscosity of liquid refrigerant. For the tube bundle, film Reynolds numbers of the tubes positioned in the first row are taken as the film Reynolds numbers for each single column.

Average HTC of the tube bundle is the area-weighted average HTCs of the outer surface of the individual tested tube in the tube bundle.

### 3.6. Uncertainty analysis

Uncertainty of calculating  $Re_f$  depends on the precision of the mass flow meter (see Table 1), uncertainty of  $\mu_1$  as well as the pressure drop between the condenser/reservoir and the evaporator. As indicated above, the difference between the two temperatures (pressure-corresponding saturation temperature and liquid temperature in reservoir) is within  $0.1^\circ\text{C}$  which suggests that the boiling process is saturation boiling. Since the measurement uncertainty of mass flow rate is negligible, the uncertainty of  $Re_f$  is subjected to the uncertainty of dynamic viscosity of liquid refrigerant which is also quite small (usually less than 2%).

Uncertainty of  $h_o$  cannot be estimated directly because the outside thermal resistance was separated from the overall thermal resistance. So the uncertainties of  $h_o$  is estimated using the method suggested in

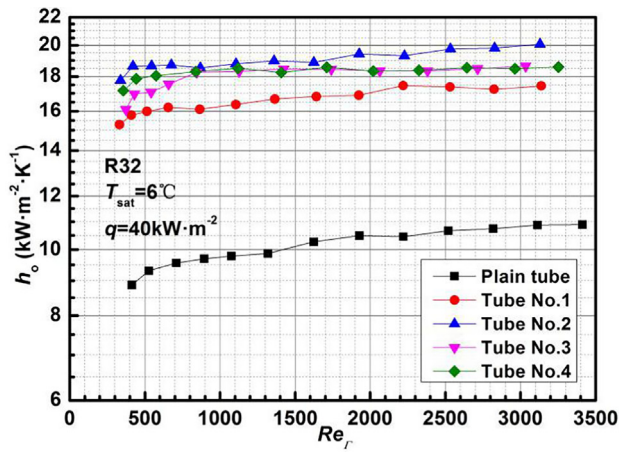
[29–32]. The estimated uncertainties of  $k$  are less than 3.5% for all test conditions. The accuracy for determining heat transfer coefficient on the tube side is quoted to be within 10% [33]. For all experimental data, the percentage of water side thermal resistance varied from 36% to 58%. Results of uncertainty analysis for  $h_o$  are shown in Table 4, and the maximum uncertainty of  $h_o$  is less than 25%.

## 4. Results and discussion

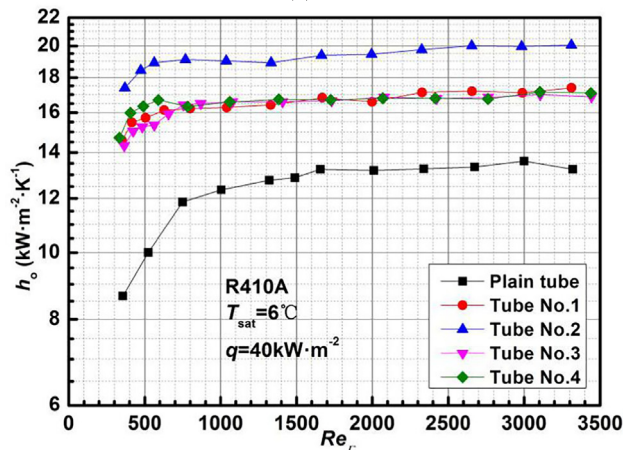
### 4.1. Water side enhanced factors

Enhanced factors of the internal surfaces were obtained by Wilson Plot Method in which the saturation temperature and heat flux are fixed and the internal water velocity is changed from 0.7 to  $3.3\text{ m}\cdot\text{s}^{-1}$ . In this study, the heat flux and saturation temperature were kept almost constant ( $q = 40 \pm 0.5\text{ kW}\cdot\text{m}^{-2}$  and  $T_{\text{sat}} = 6 \pm 0.02^\circ\text{C}$ ). For the enhanced tubes,  $k^{-1}$  vs.  $h_{\text{Gni}}^{-1}$ , is plotted and their relationship can be well described by a straight line, as seen in Fig. 5. The slope of a line is equal to  $D_o/(c_i D_i)$ , from which the enhanced factor  $c_i$  can be obtained.

Results of the single tube and the tube bundle are shown in Table 5. Since the 6 enhanced tubes in the tube bundle (tube No. 5–10) have the same enhanced structure on both sides of the tubes, the average value of their enhanced factors 3.23 is taken as the enhanced factor.



(a) R32



(b) R410A

Fig. 10. HTCs comparison among different tubes.

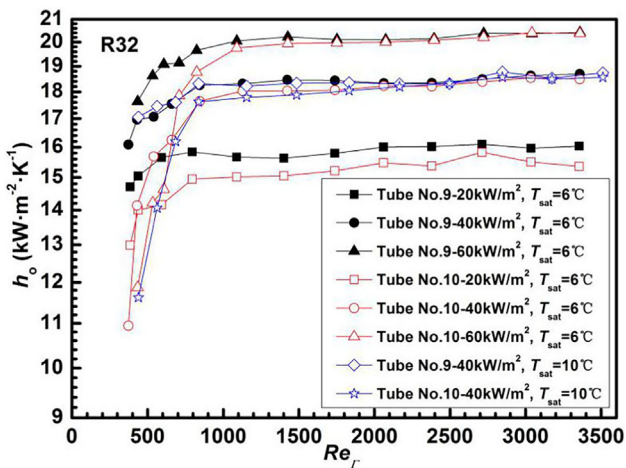


Fig. 11. HTCs of R32 on tube No. 9, 10.

#### 4.2. Falling film evaporation HTCs of the plain tube

Fig. 6 shows the results for the plain tube of two refrigerants R32 and R410A. Experiments are carried out at two saturation temperatures and three heat fluxes. For each curve, there are two obvious stages, a quasi-plateau stage at higher film Reynolds number and a sharp decrease stage when film Reynolds number is lower than a certain value. The threshold film Reynolds numbers are located from 500 to 800 for

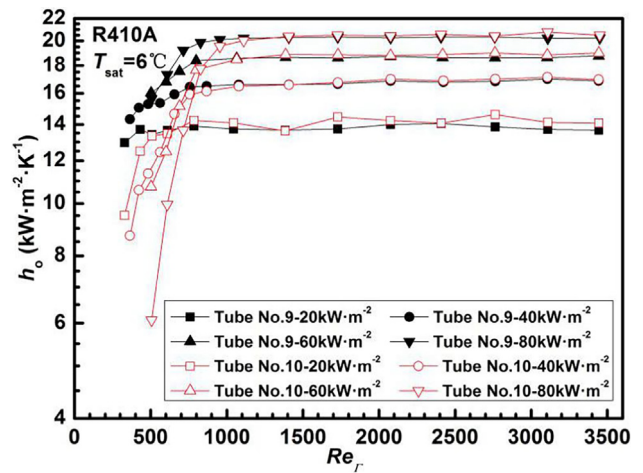


Fig. 12. HTCs of 410A on tube No. 9, 10.

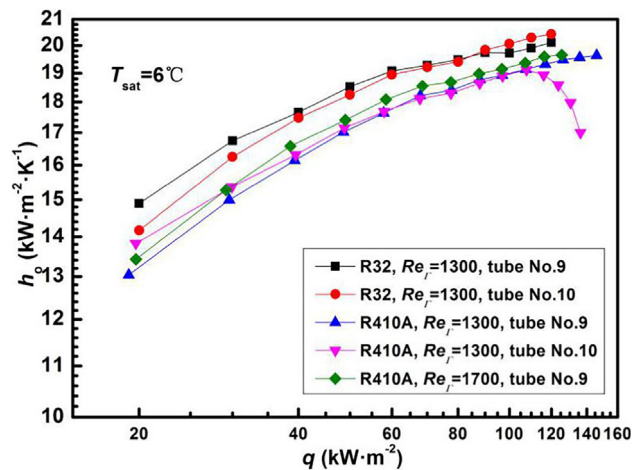
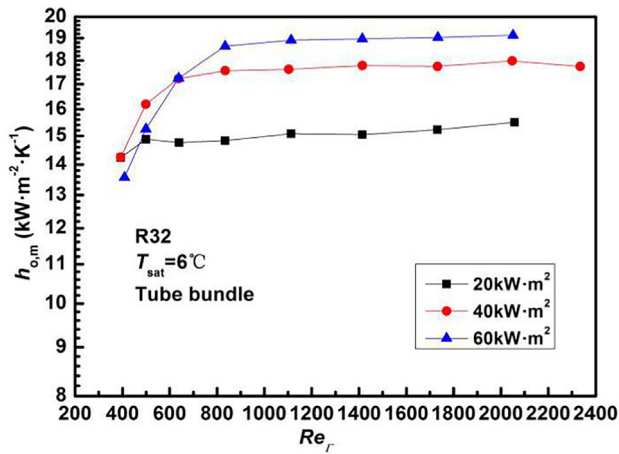


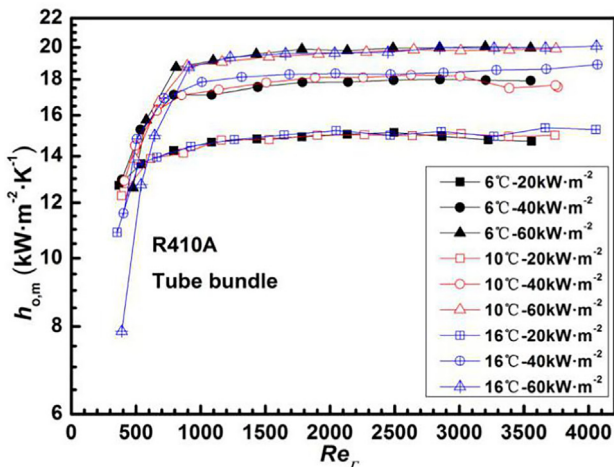
Fig. 13. Variation of HTCs with heat flux of tube No. 9, 10.

the cases studied. In addition, HTCs increase with heat flux monotonously for both refrigerants when  $T_s = 6^\circ\text{C}$ . HTCs of R410A are about 20% higher than those of R32 for each working condition. At a typical working condition of an evaporator ( $q = 40 \text{ kW}\cdot\text{m}^{-2}$ ), HTCs at saturation temperature of  $10^\circ\text{C}$  are inferior to those at  $6^\circ\text{C}$ . Comparison with the experimental results of Zhao et al. [5] shows that HTCs of R32 and R410A are all larger than those of R134a. This phenomenon can be explained by larger liquid thermal conductivity, less viscosity and larger latent heat of these two refrigerants compared with R134a.

Comparison of HTCs between falling film evaporation and pool boiling is shown in Fig. 7. For R32, results of the present study are compared with the work of Jung et al. [34] as well as Cooper's correlation [35], and we can see from the figure that HTFs of pool boiling (PB) are higher than those of falling film evaporation (FFE), and the advantage of PB increases with increase of heat flux. However, the variation trends of PB HTCs with heat flux are similar with FFE which suggests that FFE is dominated by nucleate boiling for the cases studied. Film Reynolds number has negligible influence on HTCs of falling film evaporation within the heat fluxes tested. For R410A, the present results are compared with the experimental results of Dewangan et al. [36], and similar variation trends of HTCs with heat flux are also observed, while HTCs of FFE are higher than those of PB even the pool boiling experiments were carried out on tubes with coated surfaces. It is authors' consideration that PB is very sensitive to surface condition, and the test results shown above are taken from different authors groups, hence further researches at more comparable test conditions are needed



(a) R32



(b) R410A

Fig. 14. Average HTCs of the tube bundle.

to obtain more convincing comparison results.

Zhao et al. [5] have developed two correlations considering pretty influencing factors, and achieved success in predicting HTCs with several refrigerants. Two heat transfer regimes, full wetting regime and partial dryout regime as shown in Fig. 6, are identified in their paper to predict HTCs separately. Comparison between the predictive results by Zhao's correlation of full wetting regime and the present experimental data is shown in Fig. 8. Since the criteria of  $Re_{\text{threshold}}$  in their paper cannot be applied to the present study, only the HTCs of apparent full wetting regime are compared. What should be pointed out here is that the adopted latent heat of vapor of R410A is the average value of its components R32 and R125.

It can be seen from Fig. 8 that for R32, the empirical correlation over predicts the HTCs more than 50% even up to 180%. While for R410A, the correlation can reasonably well predict the HTCs with more than 80% cases' deviation within  $\pm 30\%$ . The largest deviation happens at  $T_{\text{sat}} = 16^\circ\text{C}$  and heat flux of  $20\text{ kW}\cdot\text{m}^{-2}$ , and it may be resulted from relatively higher experimental uncertainty under this working condition. Consequently, the correlation must be studied further to extend its applicable range, including the high pressure refrigerants.

#### 4.3. Falling film evaporation HTCs on different enhanced surfaces

Fig. 9 shows the variation of HTCs of the two refrigerants with film Reynolds number and heat flux on the four types of enhanced surface. As a whole, similar with the plain tube, there are two obvious stages for each curve, especially at higher heat fluxes.

By careful expecting (inspecting) the test data, following features may be noted. First, for all enhanced tubes tested, HTCs of the refrigerants increase with heat flux, exhibiting an appreciable feature of PB; Second, at low heat flux ( $20\text{ kW}\cdot\text{m}^{-2}$ ) almost all test data of the four enhanced tubes and two refrigerants are positioned in the quasi-plateau stage, indicating that the enhanced structures are helpful to delay the occurring of partial dryout; Third, at higher heat flux for all the four enhanced tubes R410A exhibits an earlier occur of the turning point from the quasi-plateau stage to the sharp decrease stage; Fourth, as far as the values of HTCs are concerned, tube No. 2 behaves the best. Its HTCs at heat flux of  $80\text{ W}\cdot\text{m}^{-2}$  for 410A and at  $60\text{ W}\cdot\text{m}^{-2}$  for R32 are almost equal to  $24\text{ W}\cdot\text{m}^{-2}\text{ K}^{-1}$  and  $22\text{ W}\cdot\text{m}^{-2}\text{ K}^{-1}$ , respectively, being the highest HTCs in the test range of this paper.

It is interesting to compare the FFE HTCs of the smooth tube and the enhanced tubes. Fig. 10 shows the comparison of HTCs of the four enhanced tubes under a typical heat flux of  $40\text{ kW}\cdot\text{m}^{-2}$ . We can see that tube No. 2 exhibits the highest HTCs for both R32 and R410A. While tube No. 1 behaves the worst, even though for 410A, tubes No. 2 and 3 have similar heat transfer coefficients with Tube No. 1. What should be emphasized here is that tube No. 2 is designed for enhancing condensation heat transfer while performs best in the falling film evaporation process with nucleate boiling.

#### 4.4. Falling film evaporation heat transfer characteristics in a tube bundle

Experiments are also carried out for a tube bundle in staggered triangular arrangement comprised of 6 enhanced tubes as shown in Fig. 4. In the following, the HTCs of a single row (tubes No. 9, 10) are presented first and then the HTCs of the whole bundle at three heat fluxes are provided.

Fig. 11 shows HTCs of R32 for tube No. 9 and No. 10. Each curve exhibits two stages as discussed above. Under the same saturation temperature and the same nominal heat flux, HTCs of tube No. 9 are slightly higher than tube No. 10 in the full wetting regime, while in the partial dryout regime, HTCs of the lower tube decrease more sharply. The film Reynolds number of the turning points of the upper tube is a bit larger than that of the lower tube. It can also be found from Fig. 11 that the effect of saturation temperature on heat transfer is negligible for enhanced tubes. Experimental data of R410A are shown in Fig. 12. In the quasi-plateau regime the HTCs of the upper and lower tubes are almost the same, while in the partial dryout regime the lower tube exhibits an earlier turning point and a sharper decrease in HTCs.

HTC variations with heat flux for tube No. 9 and No. 10 are shown in Fig. 13. It can be found that the HTCs increase with heat flux implying nucleate boiling dominated heat transfer mode. For each tube R32 performs appreciably better than R410A, while for each refrigerant, the HTCs of the upper tube is a bit larger than those of the lower one. It worth noting that for R410A boiling on tube No. 10 at film Reynolds number of 1300 dryout occurs when heat flux is larger than  $110\text{ kW}\cdot\text{m}^{-2}$ . This is because at the same test condition, the actual film flow rate on tube No. 10 is less than that of tube No. 9, leading to an earlier occurrence of the partial dryout regime.

Tube bundle averaged HTCs of R32 and R410A are shown in Fig. 14. Two significant features may be noted. First with the increase in heat flux, both the averaged HTCs and the film Reynolds number of the turning point increase; Second the saturation temperature has negligible influence on FFE HTCs.

## 5. Conclusions

Heat transfer characteristics of falling film evaporation with nucleating boiling are experimentally studied in this paper for high pressure refrigerant R32 and R410A on four doubly enhanced tubes. The outside surface of one tube is of integrated fin while all the other three tubes have 3-D micro-fin structure. Following conclusions can be drawn:

- HTCs of falling film evaporation exhibit two fundamental stages with decrease of film flow rate, a quasi-plateau stage where film Reynolds has very mild influence on heat transfer coefficient and a sharp-decrease stage where dryout occurs because of the insufficient liquid supply.
- For both refrigerants, HTC's increase with heat flux progressively before reaching the partial dryout regime. The effect of saturation temperature on the enhanced tubes as well as the tube bundle is negligible. While for smooth tube HTC's decrease with the increase of saturation temperature.
- The integrated-fin tube performs best among the four enhanced tubes tested for both refrigerants at the typical working condition of 6 °C and 40 kW·m<sup>-2</sup>. As a whole, the HTC's of R32 are larger than those of 410A, while for the smooth tube the result is the opposite.
- Tubes positioned in the second row possess the similar variation trend of HTC's with that of the first row when no dry patches occur, however they suffer an earlier dryout because less flow rate supply compared with the upper ones.
- Correlation of Zhao et al. [5] for smooth tube can predict the experimental data of R410A of smooth tube quite reasonably with 81.3% of 91 points' deviation within ± 30%, while it appreciably over-predicts the HTC's of R32.

### Acknowledgment

This work was supported by the Foundation for Innovative Research Groups of the National Natural Science Foundation of China (No. 51721004), the Research Fund for the Doctoral Program of Higher Education of China (20120201130007), and 111 Project (B16038).

### Appendix A. Supplementary material

Supplementary data associated with this article can be found, in the online version, at <http://dx.doi.org/10.1016/j.applthermaleng.2018.03.060>.

### References

- O. Lyle, *The Efficient Use of Steam*, H.M. Stationery Office, London, 1947.
- J. Fernández-Seara, Á.Á. Pardiñas, Refrigerant falling film evaporation: description, fluid dynamics and heat transfer, *Appl. Therm. Eng.* 64 (2014) 155–171.
- G. Ribatski, A.M. Jacobi, Falling-film evaporation on horizontal tubes—a critical review, *Int. J. Refrig.* 28 (2005) 635–653.
- A.M. Abed, M.A. Alghoul, M.H. Yazdi, et al., The role of enhancement techniques on heat and mass transfer characteristics of shell and tube spray evaporator: a detailed review, *Appl. Therm. Eng.* 75 (2015) 923–940.
- C.Y. Zhao, W.T. Ji, P.H. Jin, et al., Heat transfer correlation of the falling film evaporation on a single horizontal smooth tube, *Appl. Therm. Eng.* 103 (2016) 177–186.
- Wen-Tao Ji, Chuang-Yao Zhao, Ding-Cai Zhang, et al., Effect of vapor flow on the falling film evaporation of R134a outside a horizontal tube bundle, *Int. J. Heat Mass Transf.* 92 (2016) 1171–1181.
- C.Y. Zhao, W.T. Ji, P.H. Jin, et al., Cross vapor stream effect on falling film evaporation in horizontal tube bundle using R134a, *Heat Transf. Eng.* (2017) 1–14.
- C.Y. Zhao, W.T. Ji, P.H. Jin, et al., Experimental study of the local and average falling film evaporation coefficients in a horizontal enhanced tube bundle using R134a, *Appl. Therm. Eng.* 129 (2018) 502–511.
- J.F. Roques, *Falling Film Evaporation on a Single Tube and on a Tube Bundle* (Ph.D. thesis), École Polytechnique Fédérale de Lausanne, Switzerland, 2004.
- Y. Fujita, M. Tsutsui, Experimental investigation of falling film evaporation on horizontal tubes, *Heat. Transf. Jpn. Res.* 27 (1998) 609–618.
- S.A. Moeykens, *Heat Transfer and Fluid Flow in Spray Evaporators with Application to Reducing Refrigerant Inventory* (Ph.D. thesis), Iowa State University, Iowa, USA, 1994.
- J.F. Roques, J.R. Thome, Falling films on arrays of horizontal tubes with R-134a Part I: boiling heat transfer results for four types of tubes, *Heat Transf. Eng.* 28 (5) (2007) 398–414.
- M. Habert, J.R. Thome, Falling-film evaporation on tube bundle with plain and enhanced tubes—Part I: experimental results, *Exp. Heat Transf.* 23 (4) (2010) 259–280.
- M. Christians, J.R. Thome, Falling-film evaporation on enhanced tubes, Part 1: experimental results for pool boiling, onset-of-dryout and falling film evaporation, *Int. J. Refrig.* 35 (2012) 300–312.
- M. Habert, Falling film evaporation on a tube bundle with plain and enhanced tubes (Ph.D. thesis), École Polytechnique Fédérale de Lausanne, Switzerland, 2009.
- M. Christians, *Heat transfer and visualization of falling film evaporation on a tube bundle* (Ph.D. thesis), École Polytechnique Fédérale de Lausanne, Switzerland, 2010.
- W. Li, X.Y. Wu, Z. Luo, et al., Heat transfer characteristics of falling film evaporation on horizontal tube arrays, *Int. J. Heat Mass Transf.* 54 (2011) 1986–1993.
- G.N. Danilova, V.G. Burkin, V.A. Dyundin, Heat transfer in spray-type refrigerator evaporators, *Heat Transf. Soviet Res.* 8 (1976) 105–113.
- L.H. Chien, R.H. Chen, An experimental study of falling film evaporation on horizontal tubes using R-134a, *J. Mech.* 28 (2012) 319–327.
- L.H. Chien, C. Cheng, A predictive model of falling film evaporation with bubble nucleation on horizontal tubes, *HVAC&R Res.* 12 (2006) 69–87.
- M.H. Kim, J.S. Shin, Evaporating heat transfer of R22 and R410A in horizontal smooth and microfin tubes, *Int. J. Refrig.* 28 (2005) 940–948.
- Md.A. Hossain, Y. Onaka, A. Miyara, Experimental study on condensation heat transfer and pressure drop in horizontal smooth tube for R1234ze(E), R32 and R410A, *Int. J. Refrig.* 35 (2012) 927–938.
- Md.A. Hossain, Y. Onaka, H.M.M. Afroz, et al., Heat transfer during evaporation of R1234ze(E), R32, R410A and a mixture of R1234ze(E) and R32 inside a horizontal smooth tube, *Int. J. Refrig.* 36 (2013) 465–477.
- Y. Zoua, P.S. Hrnjak, Effects of fluid properties on two-phase flow and refrigerant distribution in the vertical header of a reversible microchannel heat exchanger—comparing R245fa, R134a, R410A and R32, *Appl. Therm. Eng.* 70 (2014) 966–976.
- C.Y. Zhao, P.H. Jin, W.T. Ji, et al., Experimental investigations of R134a and R123 falling film evaporation on enhanced horizontal tube, *Int. J. Refrig.* 75 (2017) 190–203.
- S.M. Yang, W.Q. Tao, *Heat Transfer*, fourth ed., Higher Education Press, Beijing, China, 2006.
- V. Gnielinski, New equations for heat and mass transfer in the turbulent flow in pipes and channels, *Int. Chem. Eng.* 16 (1976) 359–368.
- V. Gnielinski, On heat transfer in tubes, *Int. J. Heat Mass Transf.* 63 (2015) 134–140.
- S.J. Kline, F.A. McClintock, Describing uncertainties in single-sample experiments, *Mech. Eng.* 75 (1953) 3–9.
- B. Cheng, W.Q. Tao, Experimental study of R-152a film condensation on single horizontal smooth tube and enhanced tubes, *ASME J. Heat Transf.* 116 (1994) 266–270.
- D.C. Zhang, *Experimental and numerical investigation of refrigerant condensation and boiling heat transfer characteristics on doubly-enhanced tubes* (Ph.D. thesis), School of Energy and Power Engineering, Xi'an Jiaotong University, 2007.
- Wen-Tao Ji, Ding-Cai Zhang, Ya-Ling He, et al., Prediction of fully developed turbulent heat transfer of internal helically ribbed tubes - an extension of Gnielinski equation, *Int. J. Heat Mass Transf.* 55 (2012) 1375–1384.
- Y.A. Cengel, A.J. Ghajar, *Heat and Mass Transfer, Fundamentals and Applications*, fourth ed., McGraw-Hill, New York, 2011.
- D. Jung, K. An, J. Park, Nucleate boiling heat transfer coefficients of HCFC22, HFC134a, HFC125, and HFC32 on various enhanced tubes, *Int. J. Refrig.* 27 (2004) 202–206.
- M.G. Cooper, P.H. James, F.J. Thomas, Heat flow rates in saturated nucleate pool boiling—a wide ranging examination using reduced properties, *Adv. Heat Transf.* 16 (1984) 157–239.
- A.K. Dewangan, A. Kumar, R. Kumar, Nucleate boiling of pure and quasi-azeotropic refrigerants from copper coated surfaces, *Appl. Therm. Eng.* 94 (2016) 395–403.